ChemComm

COMMUNICATION

View Article Online
View Journal | View Issue

Check for updates

Cite this: *Chem. Commun.*, 2024, **60**, 8431

Received 26th April 2024,
Accepted 15th July 2024

DOI: 10.1039/d4cc02013h

rsc.li/chemcomm

Published on 22 July 2024. Downloaded by Denison University on 9/4/2025 1:49:34 AM.

Multiple energy dissipation modes in dynamic polymer networks with neutral and ionic junctions†

Seongon Jang,[abc] Charles M. Schroeder [abcd] and Christopher M. Evans *[abc]

Polymer networks with controlled ratios of neutral and ionic dynamic crosslink points were prepared from ethylene glycol, boric acid, and lithium hydroxide. Both neutral and ionic sites led to the emergence of distinct damping modes separate from the glass transition. This work highlights the potential of polymer networks for multimodal damping spectra through dynamic bond selection.

Materials that absorb sound and energy are important for applications including shockwave dissipation, noise reduction, and impact management. Polymers have been extensively used as damping materials, where the primary dissipation process is the glass transition (T_g).[1] Near T_g, large changes in the storage (G') and loss (G'') modulus occur, and the ratio of these two parameters is the loss tangent $\left(\tan\delta = \frac{G''}{G'}\right)$. By tuning T_g, the maximum of the loss tangent shifts in frequency and can be probed by shear rheology either at a constant frequency (varying temperature) or at a constant temperature (varying frequency). The latter approach is convenient for determining the onset of substantial damping behavior at a fixed temperature, which guides materials applications.

The main approaches to tuning T_g of damping materials are through copolymerization, blending, interpenetration of networks, or plasticization.[2–4] High and low T_g monomers can be used to form statistical copolymers with a T_g depending on the overall composition that generally falls between that of the two pure homopolymers.[1,5–11] Blending of miscible polymers can also result in a material with an intermediate T_g to the two homopolymers and a controlled peak in loss tangent.[12–16] Immiscible copolymers have been formed as interpenetrating networks (IPNs) to prevent phase separation and investigated for their damping properties.[17–21] Such IPNs show enhanced dissipation relative to analogous statistical copolymers of the same composition, attributed to heterogeneity at the nanoscale. Gradient copolymers have also been investigated for damping by copolymerizing a second monomer with a syringe pump to precisely vary the monomer composition during polymerization.[7,22,23] This approach leads to polymer chains with sequence variations where the initial chain is composed primarily of one monomer and gradually transitions to monomer two. When two monomers such as *n*-butyl acrylate and styrene are used, T_gs spanning over 100 °C can be realized.

Peaks in $\tan\delta$ can arise from processes other than T_g, for example, secondary relaxations or the rubbery to flow transition.[1] Recent work has shown that networks with dynamic bonds exhibit peaks in $\tan\delta$ that arise due to the exchange process. In hydrogels with two distinct metal–ligand interactions, two damping modes were observed corresponding to the fast and slow exchanging bonds.[24,25] Two distinct damping modes can also be achieved in polymer networks with mixed hydrogen bonds and dynamic imines that exchange on timescales separated by a factor of $\approx 10^4$,[26] and this separation is retained when both bonds are incorporated into the same network. The value of the loss tangent exceeded 0.3 (a criterion for efficient damping)[19,27] for each process when the contributing dynamic bond comprised at least 50% of the crosslink points. This value is expected to vary with crosslink density but has not been systematically investigated. Interestingly, incorporating fast and slow dynamic bonds into the same network does not always lead to two damping modes. Hydrogels with slow and fast boronic esters only exhibit one damping mode.[28] In dense polymer networks with mixed boronic ester bonds, telechelic networks only show one damping mode,

[a] *Department of Materials Science and Engineering, University of Illinois Urbana-Champaign, 1304 W Green St, Urbana, Illinois, 61801, USA. E-mail: cme365@illinois.edu*
[b] *Materials Research Laboratory, University of Illinois Urbana-Champaign, 104 S Goodwin Ave, Urbana, Illinois, 61801, USA*
[c] *Beckman Institute for Advanced Science and Technology, University of Illinois Urbana-Champaign, 405 N Mathews Ave, Urbana, Illinois, 61801, USA*
[d] *Department of Chemical and Biomolecular Engineering, University of Illinois Urbana-Champaign, 600 S Mathews Ave, Urbana, Illinois, 61801, USA*

† Electronic supplementary information (ESI) available: experimental methods, synthetic procedures, and characterization. See DOI: https://doi.org/10.1039/d4cc02013h

Published on 22 July 2024. Downloaded by Denison University on 9/4/2025 1:49:34 AM.

whereas pendant crosslinked networks show two well resolved modes.[24,29]

Ionomers are another class of materials used extensively in damping applications.[30–35] The microphase separation of ionic clusters from the backbone gives rise to heterogeneity which leads to broader loss tangents and efficient dissipation. Such clusters can also exchange ionic groups, which ultimately leads to flow and a dynamic process that can lead to an increase in tan δ. Dynamic bonds bearing ionic charges have been investigated in polymer networks but not in the context of their damping performance.[36,37] The coupling of ionic interactions with bond exchange is a promising route to introduce damping modes and increase the breadth of the damping mode spectra.

Polymer networks of ethylene glycol chains with controlled ratios of neutral and ionic dynamic crosslink points were synthesized. A reaction of ethylene glycol with boric acid leads to neutral boronic esters, whereas the addition of lithium hydroxide creates anionic boronate junctions with a Li countercation. The ratio of neutral/ionic sites is determined by solid-state ^{11}B NMR, and the resulting damping properties were quantified. In neutral dynamic networks, only a single dynamic bond related damping peak is observed in addition to the peak associated with T_g. Upon the addition of ionic sites, a new damping peak emerges due to the distinct exchange rate for these sites. At the highest ionic contents (50% of the total dynamic bonds), clustering is observed *via* wide-angle X-ray scattering (WAXS), and a fourth damping mode emerges. This work demonstrates the utility of designing and preparing polymer networks with multiple dynamic bonds and ionic interactions for broad, multimodal damping spectra.

As shown in the synthetic scheme (Fig. 1), vitrimers (B-6EG-s) were synthesized by step-growth polymerization between boronic acid ($B(OH)_3$) and hexaethylene glycol (6EG). Three different vitrimer formulations were prepared by mixing $B(OH)_3$ and 6EG, while changing the ratio of neutral to ionic junctions denoted by the variable s. For instance, LiOH was added to B-6EG-25 based on this relation $\left(s = \frac{[Li^+]}{[B(OH)_3]} = 0.25\right)$, followed by adding 6EG to balance stoichiometry where each boric acid group can react with either three alcohol groups (neutral) or four alcohol/hydroxide groups (ionic). The B-6EG-25 and B-6EG-50 have 25% and 50% ionic/tetragonal crosslinking sites, compared to B-6EG-0 which has only neutral/trigonal crosslinking sites. Thermal gravimetric analysis (TGA) was performed to obtain degradation temperature (T_d, 95%) and to confirm the complete elimination of water (Fig. S1, ESI†). Each sample was heated from 30 °C to 500 °C under N_2 at 10 °C min^{-1}, and no significant mass loss was observed up to 200 °C, indicating high conversion networks with no further reactions that produce water. T_d, 95% decreased upon adding LiOH, and the residual mass at 500 °C increased due to the formation of lithium oxide. Differential scanning calorimetry (DSC) was used to determine T_g (Fig. S2, ESI†) which increased with increasing crosslinking density due to suppressed chain mobility as previously reported.[38–40] The T_gs also increased from −59 °C to −45 °C upon adding LiOH, due to the higher crosslinking density induced by ionic/tetragonal junctions. WAXS was used to investigate the nanoscale morphology after addition of LiOH (Fig. S3, ESI†). The amorphous halo (15 nm^{-1}) is observed for all vitrimers, while new peaks at 4.5 nm^{-1} and 8 nm^{-1} were observed upon adding LiOH attributed to the aggregation of ionic cross-linkers[41,42] and ions,[42,43] respectively.

The formation of the tetragonal ionic junction in the vitrimers was further confirmed by ^{11}B solid-state NMR spectroscopy (Fig. 2). A broad peak around 20 ppm was observed in neutral vitrimers corresponding to trigonal junctions (Fig. 2a). However, a sharper and higher intensity peak around 2.5 ppm emerged after the addition of LiOH, indicating the formation of ionic/tetragonal crosslinking junctions. As the ionic sites increased, the neutral sites became less prominent in the spectrum (Fig. 2b). The composition of each junction was quantitatively calculated using deconvolution analysis through MestReNova software. The neutral/trigonal and ionic/tetragonal peaks were fit using a generalized Lorentzian shape (Fig. S4, ESI†), as previously reported.[44,45] The fitted parameters are tabulated in Table S1 (ESI†), and demonstrate that the ratio of neutral/ionic junctions was controlled *via* LiOH and 6EG stoichiometry. This is essential to understanding the effects of neutral and ionic crosslinking sites on multiple energy dissipation modes. The ratio was calculated assuming the two sites have the same spin relaxation times, which may not be true in the solid states. However, the qualitative trends in ionic contents are not affected by this assumption.

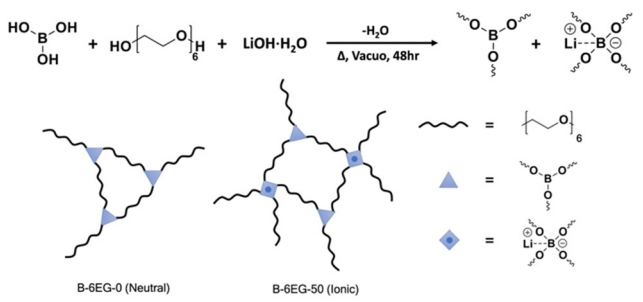

Fig. 1 Synthetic scheme for neutral/trigonal and ionic/tetragonal vitrimers.

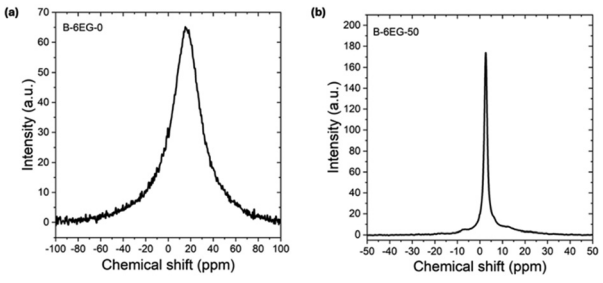

Fig. 2 ^{11}B solid-state NMR. (a) B-6EG-0 (neutral) and (b) B-6EG-50 (ionic). Two distinguishable peaks at around 20 ppm and 2.5 ppm are observed, which can be assigned to neutral and ionic boronic junctions, respectively.

 This journal is © The Royal Society of Chemistry 2024

Published on 22 July 2024. Downloaded by Denison University on 9/4/2025 1:49:34 AM.

To investigate the dynamic mechanical properties of the vitrimers, oscillatory linear viscoelastic (LVE) experiments were conducted at various temperatures. As shown in Fig. 3a, the storage (G') and loss (G'') modulus were measured from 100 rad s^{-1} to 0.01 rad s^{-1}at −20 °C (higher temperatures shown in Fig. S5, ESI†). The reciprocal of the crossover frequency (ω_c), where $G'(\omega)$ is equivalent to $G''(\omega)$, is taken as the characteristic relaxation time (τ_c). The neutral vitrimer (B-6EG-0) exhibits a Maxwellian terminal regime in which $G'(\omega) \sim \omega^2$ and $G''(\omega) \sim \omega^1$ at frequencies below $1/\tau_c$. Fig. S6a (, ESI†) also shows that a single Maxwell model can describe the relaxation behavior of the neutral vitrimer. Upon increasing ionic content to 25%, the B-6EG-25 vitrimer continues to show terminal scaling, but the rubbery plateau to flow transition is broadened and not as flat as in the neutral network. The B-6EG-50 vitrimer shows an even greater broadening of the rubber to flow transition, and a small region where G' and G'' are nearly parallel. The non-Maxwellian behavior is further highlighted in Fig. S6b and S6c (ESI†). In the ionic vitrimers, the storage modulus follows a power law behavior instead of a smooth transition from rubbery plateau to terminal regime as exhibited by many other soft materials.[46–54] Deviations from typical Maxwell behavior in the ionic vitrimers arise due to the contribution of both neutral and ionic crosslink junctions which have two distinct exchange rates, and the fact that the ionic crosslinks raise the modulus due to their higher functionality. The 50% ionic junction vitrimer (B-6EG-50) exhibits a second tan δ peak around −17 °C (Fig. 3b) with a magnitude larger than 0.5. In general, tan δ values greater than 0.3 are considered sufficient for damping in polymeric materials.[55] The T_g related damping peak is also shifted to higher temperatures for B-6EG-50. The large increase in tan δ at high temperatures arises due to the flow of the material, which is governed by the relaxation of the slower neutral site exchange process. Although minor variations in T_g values are observed from rheometery and DSC measurements, the trend of T_g is consistent for all DSC measurements.

To further investigate the relaxation modes with the introduction of ionic junctions, relaxation spectra were obtained from the oscillatory LVE experiments using TRIOS software. The relaxation time spectra over a range of temperatures between −20 °C and 40 °C are shown in Fig. 4. The frequency sweep data was fit with a regularized high-density continuous spectrum. The detailed equations for nonlinear regularization fitting are shown in the (Fig. S7, ESI†). The range of relaxation times in the spectra was determined based on guidelines given by Anderssen and Davies $\left(\frac{e^{\pi/2}}{\omega_{max}} < \tau < \frac{e^{-\pi/2}}{\omega_{min}}\right)$,[47] in addition to accounting for the normal force sensitivity (0.005 N) and diameter of rheometer plates (8 mm). As shown in Fig. 4, as temperature decreases the relaxation peaks shift to longer timescales due to slower dynamic bond exchange and segmental dynamics of polymer chains. The vitrimers with ionic junctions are shifted more than the neutral vitrimers in the same temperature range, which is also reflected in the slopes of Arrhenius plots of crossover times (Fig. S8, ESI†). Arrhenius plot slopes represent the activation energy of dynamic bond exchange and increase with more ionic junctions. These observations are attributed to the clustering of ionic sites which make bond exchange more difficult even for neutral junctions. Initially, addition of salt speeds up the crossover time due to the presence of faster exchanging ionic sites, which provide free alcohol groups to exchange with the neutral sites. Ultimately, at 50% ionic junctions, the sites begin to cluster and the crossover time increases. The relaxation time spectrum for B-6EG-50 demonstrates four distinct energy dissipation modes due to ionic junctions, although only three can be observed at a single temperature due to the frequency window of the rheology experiments. At −20 °C, the slowest relaxation time peak around 20 seconds (only partially resolved) arises due to the neutral crosslinker which accounts for the slowest process. The fastest relaxation peak around 0.1 seconds arises due to the segmental motions of the polymer chains when the temperature approaches T_g. The peak in B-6EG-50 at ∼0.4 seconds is attributed to the exchange of ionic sites. Finally, the peak at ∼3 seconds arises due to the exchange of ionic groups between aggregates which are observed in WAXS and should be slower than the exchange of the single ionic sites. Exchange times for neutral and ionic networks are found to be approximately two orders of magnitude different in the B-6EG-25 sample (Fig. S9, ESI†). Although it is difficult to resolve the presence of the ionic aggregate peak in B-6EG-25, there is a slight shoulder near 0.5 seconds in between the modes for neutral and ionic bond exchange. The neutral sites relax slower than the ionic sites based on three pieces of experimental evidence. First, the new tan δ peak with salt addition is at a lower temperature than the

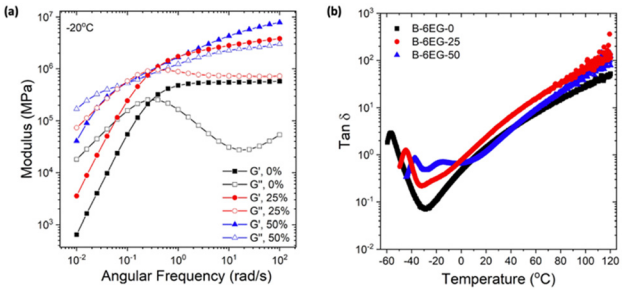

Fig. 3 Rheological characterization of boronic-ester neutral/ionic vitrimers. (a) Dynamic oscillatory linear viscoelastic measurements at 20 °C and (b) tan δ with temperature ramp.

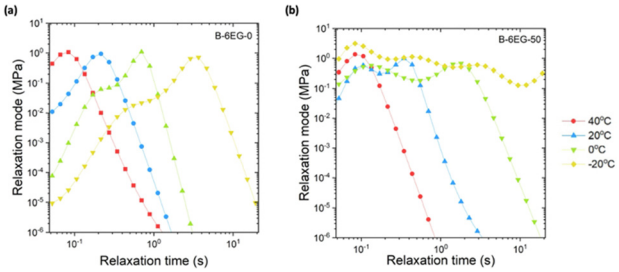

Fig. 4 Relaxation time spectra at various temperatures for boronic-ester vitrimers with different ionic junction compositions. (a) 0%, (b) 50%.

Published on 22 July 2024. Downloaded by Denison University on 9/4/2025 1:49:34 AM.

flow regime corresponding to a faster relaxation time. Second, the crossover time is similar in B-6EG-0 and B-6EG-25 (Fig. 3a) and is controlled by the neutral site exchange. Third, ionic vitrimers show increased G'' in the rubbery regime, indicating that the ionic bonds are contributing in this frequency range.

In summary, polymer networks with controlled ratios of neutral and ionic dynamic crosslinks were synthesized, and the ratio was determined using solid-state ^{11}B NMR. The resulting damping mode properties were quantified using shear rheology as a function of temperature and frequency. Networks with solely neutral dynamic bonds exhibited a single damping peak alongside the T_g peak. On the other hand, introducing ionic sites led to the emergence of a new damping peak with a distinct exchange rate and the appearance of a fourth damping mode. This study highlights the versatility of polymer networks with multiple dynamic bonds and ionic interactions in designing materials with broad, multimodal damping spectra.

The authors gratefully acknowledge the use of research facilities at Material Research Laboratory, Beckman Institute for Advanced Science and Technology, and SCS NMR Laboratory at the University of Illinois, Urbana-Champaign. This project was supported by the Air Force Office of Scientific Research, Organic Materials Chemistry Program (grant FA 9550-20-1-0262, rheological analysis, and characterization) and the National Science Foundation (NSF) *via* the Molecular Maker Lab Institute (Award 201987, NSF AI Institute, molecular design).

Data availability

The data supporting this article have been included as part of the ESI.†

Conflicts of interest

There are no conflicts to declare.

Notes and references

1 L. H. Sperling, *Sound and Vibration Damping with Polymers*, ACS Symposium Series, ACS Publications, 1990, vol. 424.
2 M.-C. O. Chang, D. Thomas and L. Sperling, *J. Polym. Sci., Part B: Polym. Phys.*, 1988, **26**, 1627–1640.
3 G. S. Huang, L. X. Jiang and Q. Li, *J. Appl. Polym. Sci.*, 2002, **85**, 746–751.
4 H. H. Chu, C. M. Lee and W. Huang, *J. Appl. Polym. Sci.*, 2004, **91**, 1396–1403.
5 J. Kenney, *Polym. Eng. Sci.*, 1968, **8**, 216–226.
6 G. Kraus, C. Childers and J. Gruver, *J. Appl. Polym. Sci.*, 1967, **11**, 1581–1591.
7 K. Sardelis, H. Michels and G. Allen, *Polymer*, 1984, **25**, 1011–1019.
8 D. Rana, H. Mounach, J. Halary and L. Monnerie, *J. Mater. Sci.*, 2005, **40**, 943–953.
9 L. Zhang, G. Liu, R. Ji, Y. Yao, X. Qu, L. Yang and J. Gao, *Polym. Int.*, 2003, **52**, 74–80.
10 M. D. Gower and R. A. Shanks, *Macromol. Chem. Phys.*, 2005, **206**, 1015–1027.
11 M. Cerrada, J. Pereña, R. Benavente and E. Pérez, *Polymer*, 2000, **41**, 6655–6661.
12 J. A. Pathak, R. H. Colby, G. Floudas and R. Jérôme, *Macromolecules*, 1999, **32**, 2553–2561.
13 C. Roland, *Rubber Chem. Technol.*, 1988, **61**, 866–878.
14 H. Cai, A. Ait-Kadi and J. Brisson, *Polymer*, 2003, **44**, 1481–1489.
15 K. Varughese, G. Nando, P. De and S. De, *J. Mater. Sci.*, 1988, **23**, 3894–3902.
16 C. Friedrich, C. Schwarzwaelder and R.-E. Riemann, *Polymer*, 1996, **37**, 2499–2507.
17 J. Fay, C. Murphy, D. Thomas and L. Sperling, *Polym. Eng. Sci.*, 1991, **31**, 1731–1741.
18 M. Chang, D. Thomas and L. Sperling, *J. Appl. Polym. Sci.*, 1987, **34**, 409–422.
19 Y. Chern, K.-H. Hsieh, C. Ma and Y. Gong, *J. Mater. Sci.*, 1994, **29**, 5435–5440.
20 N. Manoj, L. Chandrasekhar, M. Patri, B. Chakraborty and P. Deb, *Polym. Adv. Technol.*, 2002, **13**, 644–648.
21 I. Hermant, M. Damyanidu and G. Meyer, *Polymer*, 1983, **24**, 1419–1424.
22 M. M. Mok, J. Kim, C. L. Wong, S. R. Marrou, D. J. Woo, C. M. Dettmer, S. T. Nguyen, C. J. Ellison, K. R. Shull and J. M. Torkelson, *Macromolecules*, 2009, **42**, 7863–7876.
23 J. Kim, M. M. Mok, R. W. Sandoval, D. J. Woo and J. M. Torkelson, *Macromolecules*, 2006, **39**, 6152–6160.
24 S. Ge, Y.-H. Tsao and C. M. Evans, *Nat. Commun.*, 2023, **14**, 7244.
25 S. C. Grindy, R. Learsch, D. Mozhdehi, J. Cheng, D. G. Barrett, Z. Guan, P. B. Messersmith and N. Holten-Andersen, *Nat. Mater.*, 2015, **14**, 1210–1216.
26 O. R. Cromwell, J. Chung and Z. Guan, *J. Am. Chem. Soc.*, 2015, **137**, 6492–6495.
27 V. Huelck, D. Thomas and L. Sperling, *Macromolecules*, 1972, **5**, 348–353.
28 V. Yesilyurt, A. M. Ayoob, E. A. Appel, J. T. Borenstein, R. Langer and D. G. Anderson, *Adv. Mater.*, 2017, **29**, 1605947.
29 L. Porath, J. Huang, N. Ramlawi, M. Derkaloustian, R. H. Ewoldt and C. M. Evans, *Macromolecules*, 2022, **55**, 4450–4458.
30 G. Shi, X. Geng, Y. Liu and G. Wu, *Polymer*, 2024, **290**, 126543.
31 S. Jaisankar, R. M. Sankar, K. S. Meera and A. B. Mandal, *Soft Mater.*, 2013, **11**, 55–60.
32 X. Geng, G. Shi and G. Wu, *J. Appl. Polym. Sci.*, 2022, **139**, e52969.
33 T. Tomkovic and S. G. Hatzikiriakos, *J. Rheol.*, 2018, **62**, 1319–1329.
34 M. Gauthier and A. Eisenberg, *Macromolecules*, 1989, **22**, 3751–3755.
35 T. Takahashi, J. Watanabe, K. Minagawa, J.-I. Takimoto, K. Iwakura and K. Koyama, *Rheol. Acta*, 1995, **34**, 163–171.
36 M. M. Obadia, A. Jourdain, P. Cassagnau, D. Montarnal and E. Drockenmuller, *Adv. Funct. Mater.*, 2017, **27**, 1703258.
37 A. Jourdain, R. Asbai, O. Anaya, M. M. Chehimi, E. Drockenmuller and D. Montarnal, *Macromolecules*, 2020, **53**, 1884–1900.
38 J. Liu, J. J. Li, Z. H. Luo and Y. N. Zhou, *AIChE J.*, 2022, **68**, e17587.
39 Y. Liu, Z. Tang, J. Chen, J. Xiong, D. Wang, S. Wang, S. Wu and B. Guo, *Polym. Chem.*, 2020, **11**, 1348–1355.
40 J. J. Lessard, L. F. Garcia, C. P. Easterling, M. B. Sims, K. C. Bentz, S. Arencibia, D. A. Savin and B. S. Sumerlin, *Macromolecules*, 2019, **52**, 2105–2111.
41 R. G. Ricarte, F. Tournilhac and L. Leibler, *Macromolecules*, 2018, **52**, 432–443.
42 B. B. Jing, P. Mata, Q. Zhao and C. M. Evans, *J. Polym. Sci.*, 2021, **59**, 1–10.
43 U. H. Choi, Y. Ye, D. Salas de la Cruz, W. Liu, K. I. Winey, Y. A. Elabd, J. Runt and R. H. Colby, *Macromolecules*, 2014, **47**, 777–790.
44 T. Montina, P. Wormald and P. Hazendonk, *Macromolecules*, 2012, **45**, 6002–6007.
45 J. DeSilva, R. Vazquez, P. E. Stallworth, T. B. Reddy, J. M. Lehnes, R. Guo, H. Gan, B. C. Muffoletto and S. G. Greenbaum, *J. Power Sources*, 2011, **196**, 5659–5666.
46 H. H. Winter, *Structure and dynamics of polymer and colloidal systems*, ed. R. Borsali and R. Pecora, Springer, 2002, **568**, pp. 439–470.
47 A. Davies and R. S. Anderssen, *J. Non-Newtonian Fluid Mech.*, 1997, **73**, 163–179.
48 J.-T. Hang and G.-K. Xu, *J. Mech. Phys. Solids*, 2022, **167**, 104989.
49 L. E. Porath, N. Ramlawi, J. Huang, M. T. Hossain, M. Derkaloustian, R. H. Ewoldt and C. M. Evans, *Chem. Mater.*, 2024, **36**, 1966–1974.
50 R. Metzler, W. Schick, H. G. Kilian and T. F. Nonnenmacher, *J. Chem. Phys.*, 1995, **103**, 7180–7186.
51 M. Alcoutlabi and J. J. Martinez-Vega, *Polymer*, 1998, **39**, 6269–6277.
52 S. Aime, L. Cipelletti and L. Ramos, *J. Rheol.*, 2018, **62**, 1429–1441.
53 M. Bouzid, B. Keshavarz, M. Geri, T. Divoux, E. Del Gado and G. H. McKinley, *J. Rheol.*, 2018, **62**, 1037–1050.
54 R. Metzler and T. F. Nonnenmacher, *Int. J. Plast.*, 2003, **19**, 941–959.
55 G. Beniah, K. Liu, W. H. Heath, M. D. Miller, K. A. Scheidt and J. M. Torkelson, *Eur. Polym. J.*, 2016, **84**, 770–783.

 This journal is © The Royal Society of Chemistry 2024